Theor Chem Acc (2012) 131:1158
DOI 10.1007/s00214-012-1158-2

REGULAR ARTICLE

Molecular dynamics investigations of chlorine peroxide dissociation on a neural network ab initio potential energy surface

Anh T. H. Le · Nam H. Vu · Thach S. Dinh · Thi M. Cao · Hung M. Le

Received: 23 November 2011 / Accepted: 1 February 2012 / Published online: 15 February 2012

Abstract Molecular dissociation of chlorine peroxide (ClOOCl), which consists of two elementary dissociation channels (of Cl–O and O–O), is investigated using molecular dynamics simulations on a neural network-fitted potential energy surface constructed by MP2 calculations with the 6-311G(d,p) basis set. When relaxed scans of the surface are executed, we observe that Cl–O dissociation is extremely reactive with a low barrier height of 0.1928 eV (18.602 kJ/mol), while O–O bond scission is less reactive (0.7164 eV or 69.122 kJ/mol). By utilizing the "novelty sampling" method, 35,006 data points in the ClOOCl configuration hyperspace are collected, and a 40-neuron feed-forward neural network is employed to fit approximately 90% of the data to produce an analytic potential energy function. The mean absolute error and root mean squared error of this fit are reported as 0.0078 eV (0.753 kJ/mol) and 0.0137 eV (1.322 kJ/mol), respectively. Finally, quasi-classical molecular dynamics is executed at various levels of internal energy (from 0.8 to 1.3 eV) to examine the bond ruptures. The two first-order rate coefficients are computed statistically, and the results range from 5.20 to 22.67 ps^{-1} for Cl–O dissociation and 3.72–8.35 ps^{-1} for O–O dissociation. Rice-Ramsperger-Kassel theory is utilized to classically correlate internal energies to rate coefficients in both cases, and the plots exhibit very good linearity, thus can be employed to predict rate coefficients at other internal energy levels with good reliability.

Keywords ClOOCl · Chlorine peroxide · ClO dimer · Neural network · Molecular dynamics · Reaction kinetics

A. T. H. Le · N. H. Vu · T. S. Dinh · T. M. Cao · H. M. Le (✉)
Faculty of Materials Science, College of Science,
Vietnam National University, Ho Chi Minh City, Vietnam
e-mail: hung.m.le@hotmail.com

1 Introduction

The destruction of ozone has been a very important environmental issue for at least three decades because of the rapid growth of industrial manufacturers. Among the ozone destroyers, halogenated compounds are well known for their strong self-dissociation ability to yield radical products and thus lead to the destruction of ozone gas. As a result, halogenated compounds are mostly claimed as a source of potential hazard to the environmental chemistry of the stratosphere. Chlorine peroxide (ClOOCl), also known as chlorine monoxide dimer, is one particular compound of this type that has been studied by many experimentalists and theorists over the past few decades. In this work, we present a theoretical molecular dynamics (MD) study of ClOOCl dissociation at various level of internal energy on an ab initio potential energy surface (PES).

The radical species resulted from the dissociation of ClOOCl are considered as highly reactive species and have been investigated in many experimental studies. Molina and Molina [1] proposed a reaction scheme that plays an important role in the Antarctic stratosphere as follows:

$$\mathrm{ClO} + \mathrm{ClO} \xrightarrow{\mathrm{M}} \mathrm{ClOOCl} \quad (1)$$

$$\mathrm{ClOOCl} \xrightarrow{h\upsilon} \mathrm{Cl} + \mathrm{OOCl} \quad (2)$$

$$\mathrm{OOCl} \xrightarrow{\mathrm{M}} \mathrm{Cl} + \mathrm{O_2} \quad (3)$$

$$\mathrm{Cl} + \mathrm{O_3} \rightarrow \mathrm{ClO} + \mathrm{O_2}. \quad (4)$$

In that work, the compound of interest, ClOOCl, was produced in a gas-flow system in the temperature range of 220–240 K by studying collisions of atomic Cl with three different species (O_3, Cl_2O, OClO). Two major products

were witnessed to be formed during the process, which included ClOOCl and its isomer, ClOClO. In different experimental work [2], the production of ClOOCl was conducted by reacting atomic Cl with O_3, Cl_2O, OClO and atomic O with ClOCl and OClO in the presence of Ar. The temperature range of this study was somewhat similar to the previous work with an introduction of pressure control (10–30 Torr). Those halogenated radicals were in fact proved to be the main factor to cause the depletion of ozone in several particular areas and thus produced a phenomenon at the time, which is often referred to as "ozone hole" today [3, 4].

Since the concept of "ozone hole" became more familiar, this environmental subject of study has become more important and attracted attention of many environmental chemists. Under many circumstances, the breaking of ozone is more or less caused by ClO radical, and this concern has raised a critical issue regarding its dimer structure, ClOOCl, and its dissociation ability. It is of importance to evaluate the absorption cross section of ClOOCl under the photon excitation effect. Huder and DeMore [5] performed an evaluation of ClOOCl dissociation at 195 K, and the resulted photodissociation rates were approximately 40% lower than those reported by NASA earlier [6]. In the early 1990s, DeMore and Tschuikow-Roux [7] were among those who carefully characterized the reactivity of this dimer compound using spectroscopy. A first measurement of ClOOCl in the stratosphere was conducted by Stimpfle et al. [8] using the vacuum ultraviolet resonance fluorescence technique. The kinetic parameters of ClOOCl production and loss were also evaluated in the study, and they conceived good agreements with some previous literature data [3, 9]. Plenge et al. [10] performed a study in which the ClO dimer photodissociation properties were evaluated in the ultraviolet region (250 and 308 nm) under collision-free conditions. At both wavelengths, the formation of $2Cl + O_2$ was exclusively observed and the dominant yield of Cl radical product was found to be nearly unity. The loss of ClO dimer is very well known through two elementary mechanisms that we summarize below:

$$ClOOCl \xrightarrow{k_1} Cl + OOCl \quad (5)$$

$$ClOOCl \xrightarrow{k_2} ClO + OCl \quad (6)$$

These two elementary direct dissociations are reported to be the first initial step that causes such complicated reaction mechanism and leads to the destruction of ozone gas and the re-formation of ClOOCl. It is implied by Stimpfle et al. [8] that the yields of reactions 5 and 6 are approximately 0.9 and 0.1, respectively. Keeping such kinetic suggestion in mind, in this study, we perform a theoretical dynamics study of ClO dimer that leads to the formation of ClO, OOCl, and Cl radical species using ab initio molecular dynamics methods.

The recombination of two ClO molecules is believed to have a significant effect on the kinetic determination of ClOOCl dissociation. The rate of such recombination (k_{rec}) is investigated with the constrained photolysis frequency parameter, and it was observed that the concentration of ClO was significantly high [11]. In the most recent experimental study of ClOOCl, Huang et al. [12] established several detailed results that carefully characterized the formation of major products. The relative ratio of ClO:Cl was estimated to be around 0.15:1, while the ratio of $O:O_2$ was around 0.12:1, and these results consequently proved that $Cl + O_2 + Cl$ was the main dissociation process which dominantly caused the rupture of ClOOCl (with a percentage of 82%). These results again conceive reaction 5 as proposed in our scheme to dominate the dissociation of ClOOCl in the suggested elementary reaction mechanism.

In reality, ClOOCl is known to have more than one isomer. Jacobs et al. [13] conducted an investigation of Cl_2O_2 isomers using vibrational spectroscopy in cryogenic matrices. Relative energies and structures of various isomers were analyzed using DFT methods, and the authors concluded that the optimized isomer geometries were in reasonable agreement with the experimental results [14]. The relative energies resulted from DFT calculations varied by a relatively small amount of 4.5 kcal/mol depending upon the functional in use. In another theoretical study, the isomerization of ClOOCl was computed using various high-quality ab initio levels of theory (CBS-Q [15, 16], G2 [17], CBS-QB3 [18, 19], G3 [20], and G3B3 [20]), and the potential barriers of transformations among the available states were addressed by examining the intrinsic reaction coordinates [21]. In the work reported by Kaledin and Morokuma [22], direct dynamics simulations were established using the complete-active-space self-consistent field (CASSCF) method [23–28] at several levels of energy (higher than 4 eV) to study the early stage of photolysis bond breaking. The average investigated period was limited to only 10 fs, and the samples for the investigated trajectories were prepared from six initial excited stationary configurations with the non-vibrating and non-rotating considerations. Toniolo et al. [29] also presented a molecular dynamics investigation of ClOOCl at three different levels of photoexcitation (460, 325, and 264 nm) using a semiempirical force field (MNDO-d) [30] and concluded that Cl and O_2 were the main products of the photoreaction, while only a small amount of ClO was observed. In an intensive and impressive study reported by Oncak et al. [31], theoretical molecular absorption of ClO dimer was executed using five different dynamics methods that include classical and path-integral molecular

Table 1 Equilibrium bond distances and angles of ClOOCl predicted by different ab initio calculations

	Cl–O (Å)	O–O (Å)	Cl–O–O (°)	Dihedral angle (degree)
Experimental [34]	1.704	1.426	110.1	81.0
MP2/6-311G(d,p)	1.766	1.371	110.5	84.7
MP2/6-311G(2d,2p)	1.757	1.400	108.9	84.2
MP2/cc-pVTZ	1.716	1.410	109.1	83.0
B3LYP/6-311G(2d,2p)	1.811	1.325	111.8	85.5
B3LYP/cc-pVTZ	1.766	1.355	111.6	85.0
MP4(SDQ)/6-311G(2d,2p)	1.752	1.390	109.2	86.2
CCSD/6-311G(d,p)	1.761	1.367	110.3	86.4
CCSD/6-311G(2d,2p)	1.751	1.387	109.2	86.2

Table 2 Vibrational wavenumber (cm^{-1}) of ClOOCl given by different theoretical calculations

	Torsion	ClOO(s)	ClOO(as)	ClO(s)	ClO(as)	O–O
Experimental	144	325	438	539	637	755
MP2/6-311G(d,p)	130	318	433	573	628	809
MP2/6-311G(2d,2p)	124	320	433	581	641	765
MP2/cc-pVTZ	118	337	456	644	698	776
B3LYP/6-311G(2d,2p)	125	298	410	534	599	914
B3LYP/cc-pVTZ	125	323	435	547	631	853
MP4(SDQ)/6-311G(2d,2p)	124	333	441	622	653	833
CCSD/6-311G(d,p)	127	334	443	610	640	875
CCSD/6-311G(2d,2p)	122	335	444	625	657	847

dynamics. Two high-quality and very expensive ab initio methods (CASSCF and its second-order perturbation, CASPT2 [32]) were used for MD simulation.

In such a molecular system like ClOOCl, the electronic structure is somewhat complicated and requires high computational resource to perform ab initio calculations during MD simulation. The idea of executing direct dynamics in the Gaussian 03 program thus becomes unrealistic since it requires billions of ab initio calculation steps, and we believe it is more beneficial to construct a fitted PES that sufficiently describes two elementary reaction channels as showed in reactions 5 and 6 and can reproduce energy rapidly for trajectory integration. Thus, there are three major tasks in this work that are required to be deliberately executed, which includes (1) sampling the geometric data of ClOOCl in the configuration hyperspace, (2) performing an analytic fit for the potential energy with respect to input coordinates, and (3) examining ClOOCl trajectories at various levels of internal energy (with the excitation energy included) to determine the dissociation rate coefficients of Cl–O and O–O bonds.

2 Computational details

Ab initio calculations are executed using various levels of theory and basis sets in the Gaussian 03 suite of program [33], and comparisons are made to determine the most appropriate method to characterize the ClO dimer reactivity. The judgment is made based on several critical computational and theoretical issues that include computational expense and stability, convergence satisfaction of energy, and the ability to predict the reaction barrier of Cl–O bond as well as O–O bond.

In order to determine the accuracy of employed methods, we first determine the vibrational spectra of ClOOCl in accordance with the chosen levels of theory and basis sets. Our calculated equilibrium structure and vibrational wavenumbers are compared to the experimental equilibrium structure [34] and wavenumbers [12] which are all listed in Tables 1 and 2.

The calculated equilibrium structures given by B3LYP [35–38] calculations with various basis sets are not in good agreement with the experimental structure (with the percent difference of structural parameters being from 1.4 to 7.1%). In the prediction of vibrational wavenumbers, this hybrid density functional results in higher percent errors of the vibrational modes than the other calculation methods, especially the prediction of torsional and O–O stretching modes. It is admonished by Zhao and Truhlar [39] that in most cases, density functional theory (DFT) methods tend to underestimate the reaction barrier in molecular dissociation investigations. With the limitation that we have confronted when using the B3LYP functional, higher

ab initio levels of theory with reasonable computational expense are considered rather than using B3LYP.

Besides employing the DFT method, we also approach the ClOOCl molecular system using other post-Hartree–Fock methods that is believed to provide better accuracy in term of equilibrium geometry configuration and theoretical modes of vibration. When second-order Moller–Plesset perturbation (MP2) [40–44] calculations are employed with two Pople basis sets (6-311G(d,p) and 6-311G(2d,2p) [45, 46]), we conceive better agreement with the experimental data [34] in structural geometry. The predicted modes of vibration when we employ the 6-311G(d,p) and 6-311G(2d,2p) basis sets are in excellent agreement with the literature data [12] for most cases, except the symmetric vibration of Cl–O bond. The Dunning's correlation basis set [47], cc-pVTZ, does not result in good wavenumbers in comparison to the experimental results, even though it provides a very good prediction of equilibrium structure. The erroneous prediction of vibrational wavenumbers given by MP2/cc-pVTZ and B3LYP/cc-pVTZ is a consequence of inaccurate prediction of potential energy function, geometric gradients, and Hessian. Since those two calculations are approximations to the true, but unknown, wave functions, the outcome is not surprising as any given basis set fails to reproduce the experimental wavenumbers, which depends entirely upon the PES curvature at the equilibrium point. In an earlier study, Tomasello et al. [48] conducted an inspection of ClOOCl using MP2 with several basis sets (including cc-pVTZ) and reported that the PES of ClOOCl had several local minima and saddle points of different order, especially for the torsional angle of O–O bond due to instability of SCF calculations. Those results are consistent with our calculations, which show inaccuracy in predicting the torsional, symmetric, and asymmetric ClO vibrations. Moreover, the computational cost when this Dunning basis set is employed is more expensive than other basis sets [such as 6-311G(d,p)]. Consequently, the utilization of cc-pVTZ is not preferred in our study. We also extend our calculations to the fourth-order Moller–Plesset perturbation with single, double, and quadruple excitations (MP4(SDQ)) [49] and observe that the calculated results are close to the reported experimental values as shown in Tables 1 and 2.

The couple-cluster method with single and double excitations (CCSD) [50–52] is tested in this study although the utilization of this method for more than ten thousand ClOOCl configurations is unrealistic. The resulted data have shown that the CCSD method provides lower accuracy in wavenumber prediction than the cheaper computational methods such as MP2 and MP4(SDQ). We also attempt to investigate the reaction barrier of Cl–O and O–O bonds using CCSD(T) calculations, but we are unable to locate the reacting stationary point using transition state theory (TST). Most importantly, the computational time for executing one single-point energy calculation using CCSD(T) method is very high when comparing to the computational time given by other methods. Therefore, this high-level calculation is not preferred in our PES construction.

CBS-QB3 [18, 19] level of theory is employed to investigate the transition state and reaction barrier of the two reactions. In the CBS-QB3 method, stationary points are located using an optimization at the B3LYP/CBSB7 level of theory, then other calculations (CCSD(T), MP4(SDQ), and MP2) are executed at the stationary points, and the final energy is calculated from those four energies (with empirically determined coefficients). An important implication should be emphasized at this point, i.e., in CBS-QB3 calculations, transition states are predicted by a DFT functional (B3LYP), and the dissociation bond distances may not be reasonably predicted due to the critical issues of DFT methods that have been raised and discussed by Truhlar et al. [39]. According to the CBS-QB3 locations of transition states, the Cl–O and O–O bonds are believed to dissociate at 2.235 and 3.617 Å, respectively. Those predicted bond distances are higher than the values predicted by MP2 calculations, especially in the case of O–O dissociation. The predicted potential barriers are unreliable when the O–O dissociation barrier is lower than O–Cl dissociation barrier (while O–Cl dissociation has been proved experimentally to dominate the dissociation scheme). Hence, we believe that the results given by CBS-QB3 calculations are not reliable.

MP2 level of theory with the 6-311G(d,p) basis set is chosen to construct the reactive PES in this study due to its stability in predicting the reacting potential barrier when the energy with respect to the reaction coordinate is investigated. The potential energy barriers of Cl–O and O–O bond dissociations are reported in Fig. 1a, b, respectively. To produce such barriers, the bond length of interest (Cl–O or O–O) is extended with a pre-defined step size, and optimizations for transition states in Gaussian 03 [33] are employed to locate the precise transition state in term of energy. At the distance of 2.145 Å, Cl–O is believed to predominantly dissociate with a barrier height of 0.1928 eV, while it is more difficult to activate the O–O bond scission as an amount of 0.7164 eV is required. According to our transition state location, the dissociation of O–O occurs at 2.662 Å.

In most experimental studies [3, 6, 7, 12] that we have considered, it is important to emphasize again that atomic Cl and molecular O_2 are mainly produced, which implies the favor of Cl–O dissociation in the competition. The direct simultaneous dissociation of two Cl atoms can be

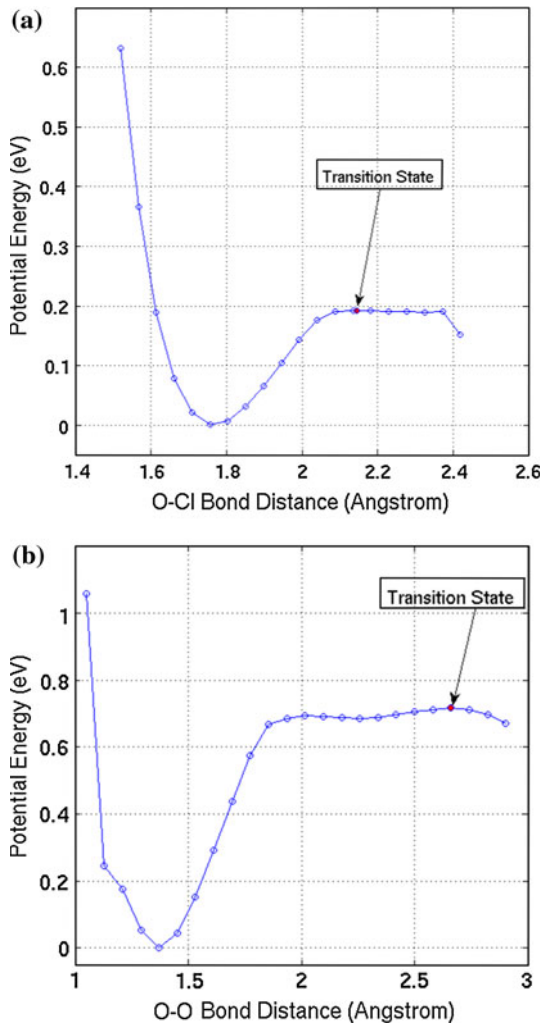

Fig. 1 **a** Potential energy barrier of Cl–O dissociation. This reaction is extremely sensitive because of its low activation energy (only 0.1928 eV or 18.602 kJ/mol), which is insignificantly higher than the ground state zero-point energy (0.1759 eV or 16.972 kJ/mol). **b** Potential energy barrier of O–O dissociation. This reaction is much less favored in the competition with Cl–O dissociation. O–O dissociation has a barrier height of 0.7164 eV (69.122 kJ/mol)

considered as a special process in the whole dissociation scheme, but the probability of this event would be small, and will not be considered in this work.

3 Construction of the potential energy surface

3.1 Neural network (NN) fitting

In this study, we employ the NN fitting technique [53] to construct a reactive PES that fully describes the two elementary reactions of interest based on the calculated MP2 energies. During the past few years, the application of NN in theoretical reaction dynamics has been proposed and vastly applied to various molecular systems. A review of the NN method in PES construction was presented by Handley and Popelier [54]. The complex molecular dissociation of six-atom vinyl bromide (CH_2CHBr) includes at least four reaction channels and thus becomes an extremely challenging task when the PES is developed. Malshe et al. [55] have demonstrated a typical study of the vinyl bromide system, in which nearly 72,000 data points were sampled, and a two-layer NN was employed to fit the PES. This approach has been further employed to investigate the reaction dynamics of SiO_2 [56], HONO [57], HOOH [58], BeH_3 [59], and O_3 [60] systems. The fitting algorithm has been improved by allowing both energies and forces (energy gradient) to be fitted, and this new application was performed in an illustrative study of H + HBr collision [61]. In a following study, the input vector optimization was investigated, in which manipulation of input was validated, and the resulted fitting accuracy was much improved without increasing the number of hidden neurons in the network [62]. Beside energy fitting, artificial NNs were also employed to fit atomic multiple moments of complex water clusters [63].

In order to produce a mathematical function that sufficiently fits the sampled data, we employ a two-layer feed-forward NN with 40 neurons in the hidden layer. The input vector introduced into the first layer comprises of six parameters, three of which represent the bond length parameters, and the other three parameters represent the cosines (cos) of two bending angles (Cl^1–O^2–O^3 and O^2–O^3–Cl^4) and one dihedral angle. Definition of the Z-matrix parameters is shown in Fig. 2. For simplicity, we denote all six parameters as r_i ($i = 1, \ldots, 6$). It is advised that the input and output values should be scaled in the range of $[-1, 1]$ to narrow the data ranges, which helps to guarantee that the entire input vector and output are unitless, and enhance fitting accuracy. The scaling formulas for input and output are as follow:

$$r_{\text{scaled}_i} = \frac{2(r_i - r_{\min_i})}{r_{\max_i} - r_{\min_i}} - 1 \tag{7}$$

$$V_{\text{scaled}} = \frac{2(V - V_{\min})}{V_{\max} - V_{\min}} - 1 \tag{8}$$

where $r_{\max_i}$ and $r_{\min_i}$ are the maximum and minimum values of the ith input value, respectively; $V_{\max}$ and $V_{\min}$ are the maximum and minimum potential energy in the database, respectively.

When we employ a two-layer feed-forward NN with 40 neurons in the hidden layer, six scaled input parameters are manipulated to produce 40 parameters that serve as inputs

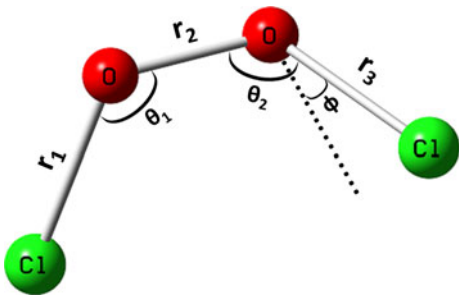

Fig. 2 Molecular structure of ClOOCl with the definition of Z-matrix parameters. In our NN input notation, $\cos\theta_1$, $\cos\theta_2$, and $\cos\phi$ are denoted as r_4, r_5, and r_6, respectively. According to our MP2 calculations, Cl–O and O–O have the equilibrium bond distances of 1.766 and 1.371 Å, respectively, while the equilibrium ClOO bending angle is 110.5°, and the equilibrium dihedral angle is 84.7°

for the second layer. The manipulation of initial inputs read:

$$n_i = f\left(\sum_{j=1}^{3} w_{j,i}^{1} r_{\text{scaled}_j} + b_i^1\right) \tag{9}$$

In this equation, w^1 is a (40 × 6) "weight" matrix, b^1 is a 40-element vector, and f is an analytic function that serves as a transfer function. In this work, we employ the hyperbolic tangent (tanh) function as a transfer function in the first layer.

Those 40 calculated n values are used to produce an output value which represents the scaled potential energy (unitless), which is later converted to the potential energy (in eV) by manipulating Eq. 8. Quite similarly to the calculations in the first layer, the scaled output is then calculated with only one distinction of the transfer function being a linear function. The equation to calculate the scaled potential energy is as below:

$$V_{\text{scaled}} = \sum_{i=1}^{60} w_i^2 n_i + b \tag{10}$$

w^2 and b are a 40-element vector and a real number constructing the second layer, respectively.

In our training process, the analytic fit is produced by fitting approximately 90% of the sampled data using the Levenberg–Marquardt algorithm [53], while the other 5% of data serve as the testing set, and the remaining data constitute the validation set. In total, if no convergence criteria are satisfied, 1,000 epochs (training iterations) will be executed. The purpose of utilizing a validation set is to prevent a common problem in machine-learning algorithm often referred to as over-fitting [64]. In most cases, over-fitting is a consequence of using an excessive number of neurons in the hidden layer. Empirically, it is realized that if the error of the validation set increases continuously, over-fitting begins to occur. In order to prevent over-fitting, when the error of the validation set increases in 6 consecutive epochs, the training process is terminated, and all optimized coefficients are reported before the increase in validation set error occurs.

3.2 Novelty sampling of configurations in multi-dimensional hyperspace

The PES construction requires an efficient sampling procedure [55–57, 65] to sufficiently select data points from the multi-dimensional hyperspace. A particular construction of the NN PES perhaps requires more configurations to be selected than the other PES fitting methods. There are at least two major sampling strategies that have been developed during the past recent years; one of which employs MD trajectories on a temporary PES to sample configurations, and the other method samples data with an analysis of input gradients and is independent of MD trajectories. The former method, which is well known as "novelty sampling," is employed with some modifications in our study to collect data point, while the other method is termed "gradient sampling" [58].

In general, the novelty sampling procedure is an iterative operation of MD trajectories to generate new configuration points. Traditionally, a first set of data is initially generated by either performing MD trajectories on a pre-constructed empirical PES or executing direct dynamics [66]. In this study, we construct a first set of data points using relaxed scans of input parameters in Gaussian 03, and then, a temporary PES is constructed by fitting the obtained data points. Subsequently, MD trajectories are performed on the temporary PES that allows us to select more configuration points to add to the database, and an updated NN fit is performed. This process is done iteratively until some convergence criteria are met (those criteria will be discussed later).

A first set of data is prematurely generated by performing five relaxed scans of the PES with various constraints being applied during the scanning process. The two chemical bonds in concern (Cl–O and O–O) are first optimized with various values, and the other five input parameters are fully relaxed using the steepest descent algorithm. Subsequently, three more relaxed scans are executed with the variations of the dihedral angle and one of the remaining input parameters (Cl–O or O–O bond or Cl–O–O bending angle), while the rest are fully relaxed. This procedure results in an initial data set of 998 configurations with the upper limit of 1.2 eV in energy. The choice of this maximum energy is meaningful to construct a PES with high fitting accuracy, which is obligated to describe the low reaction barrier of Cl–O as previously discussed in Fig. 1a. The data are then scaled using Eqs. 7

Table 3 Minimum and maximum values of parameters in the database

	O–Cl bond (Å)	O–O bond (Å)	cos(θ) (Cl–O–O angle)	cos(ϕ) (dihedral angle)	Potential energy (eV)
Minimum	1.481	1.048	−1.000	−1.000	0.000
Maximum	2.449	2.823	0.282	1.000	1.200

and 8 with the maximum and minimum input parameters provided in Table 3, and the distances between all pairs of scaled data points are then calculated (shown in Eq. 11 below). 998 minimum distances are found, every single one of which confines the smallest distance from one particular configuration to the remaining configurations. The average of those minimum distances is finally computed by taking the average of 998 minimum distances above, and the resulted value is given as 0.0817. This average minimum distance value is used in our sampling "novelty sampling" procedure.

After the construction of the first data set, we perform a NN fit with 40 neurons in the hidden layer to construct a temporary PES. In general, when a PES function is fitted, symmetry consideration is taken into account due to the symmetric property of the molecule; therefore, with an initial set of 998 points, we need to perform a NN fit for 1,996 points. Finally, MD trajectories at the total internal energy of 0.176 eV (equal to the zero-point energy of ClOOCl) are executed, and more configurations are generated. To evaluate data distribution in the configuration hyperspace, we introduce a new quantity, which is the distance between data points A and B. The distance is computed using scaled input parameters as follow:

$$d_{AB} = \sqrt{\sum_{i=1}^{6} (r_{A\_scaled_i} - r_{B\_scaled_i})^2}. \quad (11)$$

New generated configurations are selected if they qualify all these following criteria:

1. The distances to every existing configuration in the database are larger than 0.0817. This distance criterion guarantees the uniform distribution of data in the hyperspace.
2. Every element of the scaled input vector of the new configuration is in the pre-defined range of [−1, 1].

The NN-predicted potential energies in correspondence with the selected configurations are calculated and stored in the database for the later qualification examination. MP2 calculations are executed, and the resulted ab initio energies are then compared with the NN-predicted energies. A final qualification judgment is made before adding a configuration into the database by examining the absolute difference between its real ab initio and NN energies. If the absolute difference is larger than 0.01 eV, the new configuration is selected; otherwise, it will be eliminated. This last criterion helps to disqualify those configurations that are already well described by the NN, and their participation in the database would cause bad fitting in the other regions. After selecting all qualified configurations, we perform a new NN fit to produce a new and updated PES.

Such procedure is employed to select more configurations iteratively to be added to the database. In iteration 2, more data points are sampled using MD trajectories at the total internal energies of 0.176 eV in order to fully characterize the ground state vibrations of ClOOCl.

After executing two sampling iterations, the total energy for sampling is increased up to 1.5 eV to obtain more data in the reactive regions. Those later steps strongly focus on the important stretching of Cl–O and O–O. Additional iterations are required to sample data, which increases the total number of iterations to 16, until the convergence criteria are closely attained (as shown by the detailed numbers of data points in Table 4). In the last iterations, we can only obtain 321 points from MD trajectories, and only 133 are finally selected (41.4%). At this stage, we decide to terminate the sampling process as the database has converged and the latest NN PES is believed to fully describe the reacting behaviors of two chemical bonds. In total, we have collected 17,503 configurations to construct the PES of ClOOCl system. The database is later duplicated using the symmetric consideration, which consequently increases the total number of data points to 35,006 points.

3.3 Quality of the fitted PES

The NN fitting algorithm in Matlab [67] is employed to fit approximately 90% of 35,006 data points. The resulted mean absolute error and root mean squared error are 0.0078 eV (0.753 kJ/mol) and 0.0137 eV (1.322 kJ/mol), respectively, which reveal excellent fitting accuracy.

The ratio between root mean squared error and mean absolute error is almost 1.8, which implies the existence of a minority of bad-fitting data points. However, the contribution of these errors is insignificant and does not have a big effect on the quality of the fitted PES. In Fig. 3a, a plot of real ab initio energies versus NN-predicted energies is shown. A better implication of the domination of well-fitted data points is illustrated in Fig. 3b, in which we can see a very large number of small fitting errors in

Table 4 Number of data points obtained and selected in every iteration

Iteration	Points obtained	Points selected	Percent of selection	Points in database	Note
0				998	
1	1,418	885	62.4	1,883	Sampling at zero-point energy
2	2,027	2,021	99.7	3,904	
3	3,172	2,502	78.9	6,406	Sampling at 1.5 eV of internal energy
4	2,559	1,823	71.2	8,229	
5	1,815	1,249	68.8	9,478	
6	1,554	1,047	67.4	10,525	
7	1,892	1,233	65.2	11,758	
8	1,761	1,096	62.2	12,854	
9	1,501	959	63.9	13,813	
10	1,515	618	40.8	14,431	
11	3,692	1,362	36.9	15,793	
12	1,156	485	42.0	16,278	
13	1,079	437	40.5	16,715	
14	855	409	47.8	17,124	Focusing more on O–O stretching
15	515	246	47.8	17,370	
16	321	133	41.4	17,503	

comparison to a much smaller number of large fitting errors. The domination of small fitting errors constitutes excellent fitting accuracy as reported previously.

4 Molecular dynamics of Cl–O and O–O dissociations

The chemical reactions of interest in this study are two first-order reactions, and the rate coefficients of which change when the internal energy is varied. In order to determine the rate coefficients with good statistical accuracy, the task in our MD simulations is to accurately determine the reaction period when a chemical reaction occurs. The reaction time is recorded and used for later determination of the rate constants k_1 and k_2 as shown in chemical reactions 5 and 6.

Prior to conducting MD simulations, a configuration with randomized geometry and Cartesian momenta must be prepared. Initially, the Cartesian coordinates of ClOOCl equilibrium structure is assigned, and we introduce the ground state vibrational energy (0.176 eV) into each vibrational mode using the projection method developed by Raff [68]. The trajectory is integrated for a randomized period of time (between 0 and twice the longest vibrational period). After this short integration, the excitation energy is introduced into the vibrational modes equally using the projection method. At this point, a well-randomized configuration with the excitation energy included is prepared for trajectory investigation.

The quasi-classical MD simulations are utilized to perform trajectory calculations for the ClOOCl molecular system. The fourth-order Runge–Kutta method with a fixed step size of 1.018×10^{-16} s is employed to numerically integrate 24 partial differential equations simultaneously. It is required that the total angular momentum should vanish during the entire trajectory.

Five levels of internal energy (including zero-point energy) are investigated, which are 0.8, 1.0, 1.1, 1.2, and 1.3 eV. In each case, 1,000 sample trajectories are investigated. During the trajectory, we monitor the O–O bond and two Cl–O bonds at every integration step to examine the occurrence of chemical reactions. If one of the Cl–O bonds is greater than 2.145 Å and the energy gradient with respect to the O–Cl distance is negative, the trajectory is terminated and the reaction time of Cl–O dissociation is recorded. Similarly, when the O–O distance is greater than 2.662 Å and the energy gradient with respect to the O–O distance is negative, we conclude the reaction to be O–O dissociation and record its reaction time.

5 Results and discussion

As previously mentioned in this paper, the two reactions of interest are of first-order type, where Cl–O bond scission is much more sensitive than other one. At the investigated internal energies, we observe that Cl–O dissociation greatly dominates in the product yield, and this domination even rises significantly as the internal energy increases as shown in Fig. 4. In most cases, we see that the yield of Cl–O dissociation dominantly occupies 80–90% of 1,000

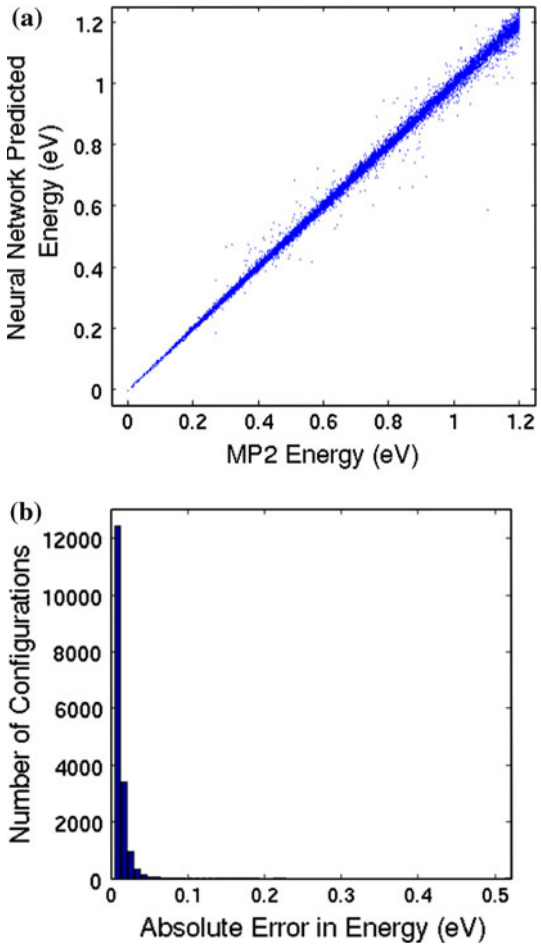

Fig. 3 **a** Plot of calculated MP2 energies versus NN-predicted energies. **b** Distribution of the absolute errors when the NN fit is applied to all configurations in the database. A majority domination of small fitting errors can be easily observed in this plot

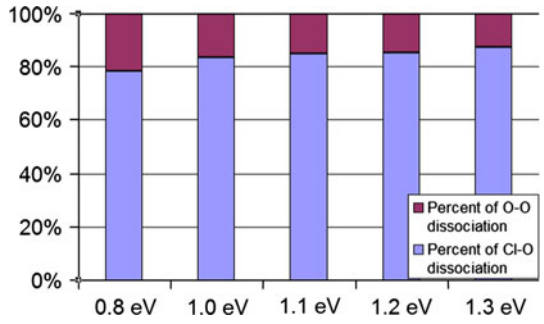

Fig. 4 Percentage of Cl–O and O–O dissociations at various levels of internal energy. Note that the reactant samples are all consumed to yield products in all cases

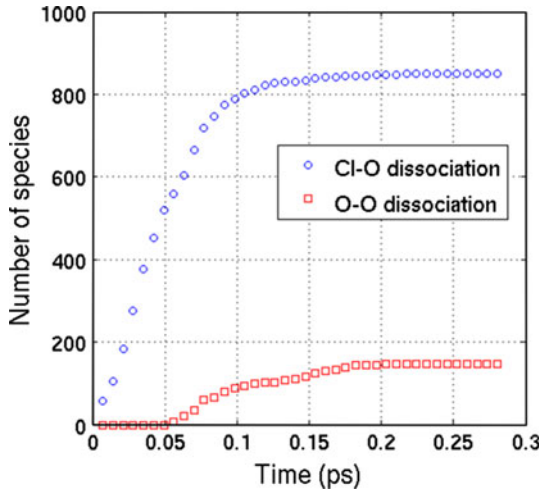

Fig. 5 Number of O–Cl and O–O dissociation species (over 1,000 samples) with respect to time at 1.2 eV internal energy

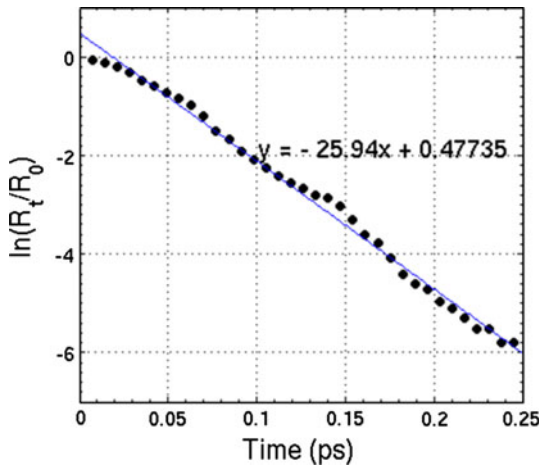

Fig. 6 First-order decay plot of the initial reactant (ClOOCl) at the internal energy of 1.2 eV. The plot exhibits very good linearity, and the sum of two rates $(k_1 + k_2)$ can be extracted with good statistical accuracy

investigated samples. The greater domination observed in this study agrees well with an implication in the literature [8]. Even though these two reactions are competitive against each other, the linear combination of these two reactions yields a first-order decay of the initial reactant ClOOCl. Therefore, the mathematical decay rate of ClO-OCl concentration reads:

$$\frac{\mathrm{d}[\mathrm{ClOOCl}]}{\mathrm{d}t} = -(k_1 + k_2)[\mathrm{ClOOCl}]. \quad (12)$$

According to the above equation, the sum of two rate constants at a certain investigated internal energy level can be determined by making a first-order decay plot of the initial reactant concentration. In Fig. 6, an illustrative example is shown for the 1.2 eV internal energy case, and the extracted $(k_1 + k_2)$ is 25.59 ps^{-1} from the linear fit. Recall that the chosen internal energy levels in all cases

Table 5 Calculated rate constants of Cl–O and O–O dissociations at various levels of internal energy

Internal energy (including zero-point energy) (eV)	Total rate ($k_1 + k_2$) (ps^{-1})	Ratio (k_2/k_1)	Cl–O dissociation rate (k_1) (ps^{-1})	O–O dissociation rate (k_2) (ps^{-1})
0.8	8.92	0.71	5.20	3.72
1.0	17.18	0.57	10.95	6.23
1.1	21.37	0.51	14.12	7.25
1.2	25.94	0.48	17.51	8.43
1.3	31.02	0.37	22.67	8.35

(0.8 eV and above) are sufficient to activate the reaction barriers of both reactions (Fig. 5).

It is important to imply again that the considered reactions in this study are both first order; thus, in reality, the number of Cl–O dissociations is directly proportional to the number of O–O dissociations at any point of time. Hence, the statistical ratio of O–O dissociation species and Cl–O dissociation species must be k_2/k_1. Therefore, in order to determine k_1 and k_2 individually, we need to determine average statistical ratio of the two reaction species.

When classical dynamics is utilized to treat the system, unfortunately, the reaction profile is not as novel as we have expected, and the above implication is not quite true. Energetically, Cl–O dissociation is much easier to occur than the other reaction and its rate is extremely rapid in the very first reaction stage. We can only witness the evidence of O–O dissociation after a certain period of time. To clarify this statement, we present the product count of Cl–O and O–O dissociations with respect to time in Fig. 5, and it can be seen that during the initial 0.05 ps timeframe, no evidence of O–O dissociation is found.

Neglecting the classical issue discussed above, we can still roughly determine the ratio of k_2/k_1 by ignoring the special timeframe without observation of O–O dissociation, and we only consider the later time period when both reactions involve. Adopting this particular assumption, we compute the k_2/k_1 ratio and extract rate constants k_1 and k_2 for each level of internal energy as shown in Table 5.

The rate coefficient of Cl–O dissociation varies from 5.20 to 22.27 ps^{-1} as the internal energy is varied from 0.8 to 1.3 eV, while O–O dissociation rate coefficient ranges from 3.72 to 8.35 ps^{-1}. The O–O dissociation probability tends to decrease with the increment of internal energy. At 0.8 eV of internal energy, we observe the highest rate constant ratio of k_2/k_1 (0.71), while this ratio takes the lowest values when the internal energy is 1.3 eV. This result makes sense in the classical manner because Cl–O dissociation rate would be further enhanced due to its high reactivity. At the highest investigated energy, k_1 is almost 3 times k_2; however, at the lowest investigated energy level, the difference between the two rates is insignificant.

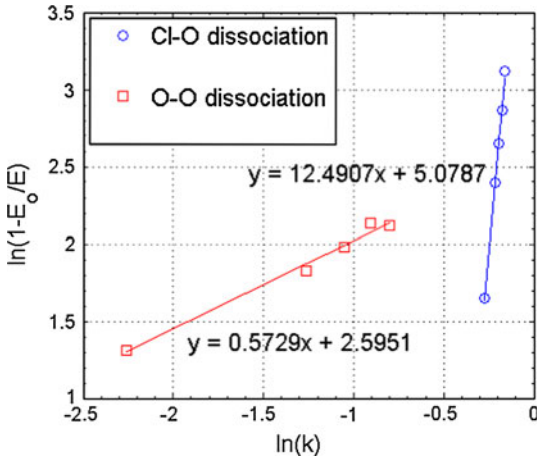

Fig. 7 Logarithm correlations of O–Cl and O–O dissociation rate coefficients to the internal energies using the Rice-Ramsperger-Kassel expression

The resulted first-order rate coefficients of two dissociations are then correlated to internal energies using the Rice-Ramsperger-Kassel (RRK) equation:

$$\ln(k) = \ln(f) + (s-1)\ln\left(1 - \frac{E_0}{E}\right) \tag{13}$$

where E_0 is the reaction barrier of Cl–O bond or O–O bond, and E is the internal energy. The equations for two linear fits are shown in Fig. 7. The linearity in both plots is very good which reveals a reliable correlation between the total internal energy and rate coefficient of the two reactions when RRK theory is adopted. Therefore, two energy-dependent rate coefficients can be demonstrated as two functions of total internal energy as shown in Eqs. 14 and 15 below:

$$k_1(E) = 160.57 ps^{-1}\left(1 - \frac{0.1928\,eV}{E}\right)^{5.079} \tag{14}$$

$$k_2(E) = 13.40 ps^{-1}\left(1 - \frac{0.7164\,eV}{E}\right)^{0.573}. \tag{15}$$

In the above RRK equations, we see that the f value for Cl–O dissociation is extremely high, while the f value for O–O dissociation is much lower. Classically, with an s value of 6.079, the RRK theory suggests that all six

vibrational modes effectively participate in the dissociation process, while in the O–O case, less than two vibrational modes involve in the bond dissociation ($s = 1.573$). These two RRK equations with the resulted parameters can be employed to predict other rate coefficient when an internal energy of the system is given.

6 Summary

We present in this study a classical MD simulation of chlorine peroxide dissociation in gas phase on a NN ab initio PES at various levels of internal energy. Different levels of ab initio theories are executed to predict the equilibrium configuration and vibrational wave numbers of ClOOCl as well as the potential barrier of Cl–O and O–O dissociations. Those ab initio methods include B3LYP, MP2, MP4(SDQ), and CCSD. Among them, MP2/6-311G(d,p) gives the most accurate result in structural and vibrational analysis and establishes numerical stability in predicting the reaction barrier. Therefore, this method is chosen to perform ab initio calculations of potential energy. According to our MP2 calculations, the barrier heights of Cl–O and O–O dissociations are 0.1928 eV (18.602 kJ/mol) and 0.7164 eV (69.122 kJ/mol), respectively.

In total, we have collected 35,006 data points in the configuration hyperspace using the novelty sampling procedure, and the corresponding MP2 energies are calculated. To construct the PES, we employ a two-layer feed-forward NN with 40 neurons in the hidden layer to numerically fit MP2 energies as a function of the input parameters. We have chosen to loosen the upper limit of energy in order to achieve better fitting accuracy, which is indispensably required in this study because of the sensitivity of Cl–O dissociation (with the barrier being only 18.602 kJ/mol). The resulted mean absolute error and root mean squared error in this work are given as 0.0078 eV (0.753 kJ/mol) and 0.0137 eV (1.322 kJ/mol), respectively.

MD trajectories of ClOOCl are executed at different levels of internal energy (including zero-point energy), which are 0.8, 1.0, 1.1, 1.2, and 1.3 eV. In each trajectory, we monitor three chemical bonds carefully to examine the dissociation time and rate. It is observed in all trajectories that molecular dissociation of this chlorinated compound occurs extremely fast. Cl–O dissociation is believed to dissociate with much greater yield (80–90% of 1,000 samples in total) according to our reaction profile, and this conceives a good agreement with the experimental suggestion [8].

The investigated dissociations are two first-order reactions, and the rate coefficients are determined in this study (as showed in Table 5). At lower internal energy levels, higher ratio of k_2/k_1 is observed, and the ratio tends to decrease as we increase the total energy.

The resulted rate coefficients for both reactions are fitted to the RRK equation in correspondence with the internal energies, and we conceive good linearity in both cases. As the proof of good statistical correlation is presented, the established RRK equations can be utilized to predict the first-order rate constants at other internal energy levels.

Acknowledgments We thank Prof. Lionel M. Raff from the Chemistry Department, Oklahoma State University for his helpful advice in this research. The authors also thank the Faculty of Materials Science, College of Science, Vietnam National University (VNU) in Ho Chi Minh City for their computing supports. The research grant for this work is funded by VNU.

References

1. Molina LT, Molina MJ (1987) Production of chlorine oxide (Cl_2O_2) from the self-reaction of the chlorine oxide (ClO) radical. J Phys Chem 91(2):433–436
2. Cheng B-M, Lee Y-P (1989) Production and trapping of gaseous dimeric ClO: the infrared spectrum of chlorine peroxide (ClO-OCl) in solid argon. J Chem Phys 90(11):5930–5935
3. Cox RA, Hayman GD (1988) The stability and photochemistry of dimers of the ClO radical and implications for Antarctic ozone depletion. Nature 332(6167):796–800
4. Barrett JW, Solomon PM, de Zafra RL, Jaramillo M, Emmons L, Parrish A (1988) Formation of the Antarctic ozone hole by the CIO dimer mechanism. Nature 336(6198):455–458
5. Huder KJ, DeMore WB (1995) Absorption cross sections of the ClO dimer. J Phys Chem 99(12):3905–3908
6. Demore WB, Golden DM, Hampson RF, Howard CJ, Kolb CE, Kurylo MJ, Molina MJ, Ravishankara AR, Sander SP (1997) Chemical kinetics and photochemical data for use in stratospheric modeling. JPL Publication, Vol 94-26. Jet Propulsion Laboratory, California Institute of Technology, Pasadena, CA
7. DeMore WB, Tschuikow-Roux E (1990) Ultraviolet spectrum and chemical reactivity of the chlorine monoxide dimer. J Phys Chem 94(15):5856–5860
8. Stimpfle RM, Wilmouth DM, Salawitch RJ, Anderson JG (2004) First measurements of ClOOCl in the stratosphere: the coupling of ClOOCl and ClO in the Arctic polar vortex. J Geophys Res 109(D3):D03301
9. Avallone LM, Toohey DW (2001) Tests of halogen photochemistry using in situ measurements of ClO and BrO in the lower polar stratosphere. J Geophys Res 106(D10):10411–10421
10. Plenge J, Flesch R, Kühl S, Vogel B, Müller R, Stroh F, Rühl E (2004) Ultraviolet photolysis of the ClO Dimer. J Phys Chem A 108(22):4859–4863
11. Sumińska-Ebersoldt O, Lehmann R, Wegner T, Grooß JU, Hösen E, Weigel R, Volk CM, Borrmann S, Rex M, Stroh F, von Hobe M (2011) ClOOCl photolysis at high solar zenith angles: analysis of the RECONCILE self-match flight. Atmos Chem Phys Discuss 11(7):18901–18926
12. Huang W-T, Chen AF, Chen IC, Tsai C-H, Lin JJ-M (2011) Photodissociation dynamics of ClOOCl at 248.4 and 308.4 nm. Phys Chem Chem Phys 13(18):8195–8203
13. Jacobs J, Kronberg M, Mueller HSP, Willner H (1994) An experimental study on the photochemistry and vibrational spectroscopy of three isomers of Cl_2O_2 isolated in cryogenic matrixes. J Am Chem Soc 116(3):1106–1114

14. Han Y-K, Kim KH, Lee YS, Baeck KK (1998) Energies and structures of isomers of Cl_2O_2 calculated by density functional methods. J Mol Struct THEOCHEM 431(1–2):185–189
15. Ochterski JW, Petersson GA, Montgomery JA (1996) A complete basis set model chemistry. V. Extensions to six or more heavy atoms. J Chem Phys 104(7):2598–2619
16. Petersson GA, Tensfeldt TG, Montgomery JA (1991) A complete basis set model chemistry. III. The complete basis set-quadratic configuration interaction family of methods. J Chem Phys 94(9):6091–6101
17. Curtiss LA, Raghavachari K, Trucks GW, Pople JA (1991) Gaussian-2 theory for molecular energies of first- and second-row compounds. J Chem Phys 94(11):7221–7230
18. Montgomery JA, Frisch MJ, Ochterski JW, Petersson GA (1999) A complete basis set model chemistry. VI. Use of density functional geometries and frequencies. J Chem Phys 110(6): 2822–2827
19. Montgomery JA, Frisch MJ, Ochterski JW, Petersson GA (2000) A complete basis set model chemistry. VII. Use of the minimum population localization method. J Chem Phys 112(15):6532–6542
20. Baboul AG, Curtiss LA, Redfern PC, Raghavachari K (1999) Gaussian-3 theory using density functional geometries and zero-point energies. J Chem Phys 110(16):7650–7657
21. Jalbout AF (2002) The isomerization of ClOOCl: high level ab initio and density functional theory analysis. J Mol Struct THEOCHEM 594(1–2):1–7
22. Kaledin AL, Morokuma K (2000) An ab initio direct-trajectory study of the photodissociation of ClOOCl. J Chem Phys 113(14):5750–5762
23. Hegarty D, Robb MA (1979) Application of unitary group methods to configuration interaction calculations. Mol Phys 38(6):1795–1812
24. Eade RHA, Robb MA (1981) Direct minimization in mc scf theory. The quasi-newton method. Chem Phys Lett 83(2): 362–368
25. Schlegel HB, Robb MA (1982) MC SCF gradient optimization of the H_2CO–>H_2+CO transition structure. Chem Phys Lett 93(1):43–46
26. Bernardi F, Bottoni A, McDouall JJW, Robb MA, Schlegel HB (1984) MCSCF gradient calculation of transition structures in organic reactions. Faraday Symp Chem Soc 19:137–147
27. Frisch M, Ragazos IN, Robb MA, Bernhard Schlegel H (1992) An evaluation of three direct MC-SCF procedures. Chem Phys Lett 189(6):524–528
28. Yamamoto N, Vreven T, Robb MA, Frisch MJ, Bernhard Schlegel H (1996) A direct derivative MC-SCF procedure. Chem Phys Lett 250(3–4):373–378
29. Toniolo A, Granucci G, Inglese S, Persico M (2001) Theoretical study of the photodissociation dynamics of ClOOCl. Phys Chem Chem Phys 3(19):4266–4279
30. Dewar MJS, Thiel W (1977) Ground states of molecules. 38. The MNDO method. Approximations and parameters. J Am Chem Soc 99(15):4899–4907
31. Oncák M, Sistík L, Slavícek P (2010) Can theory quantitatively model stratospheric photolysis? Ab initio estimate of absolute absorption cross sections of ClOOCl. J Chem Phys 133(17): 174303
32. Finley J, Malmqvist P-Å, Roos BO, Serrano-Andrés L (1998) The multi-state CASPT2 method. Chem Phys Lett 288(2–4):299–306
33. Frisch MJ, Trucks GW, Schlegel HB, Scuseria GE, Robb MA, Cheeseman JR, Montgomery Jr JA, Vreven T, Kudin KN, Burant JC, Millam JM, Iyengar SS, Tomasi J, Barone V, Mennucci B, Cossi M, Scalmani G, Rega N, Petersson GA, Nakatsuji H, Hada M, Ehara M, Toyota K, Fukuda R, Hasegawa J, Ishida M, Nakajima T, Honda Y, Kitao O, Nakai H, Klene M, Li X, Knox JE, Hratchian HP, Cross JB, Bakken V, Adamo C, Jaramillo J, Gomperts R, Stratmann RE, Yazyev O, Austin AJ, Cammi R, Pomelli C, Ochterski JW, Ayala PY, Morokuma K, Voth GA, Salvador P, Dannenberg JJ, Zakrzewski VG, Dapprich S, Daniels AD, Strain MC, Farkas O, Malick DK, Rabuck AD, Raghavachari K, Foresman JB, Ortiz JV, Cui Q, Baboul AG, Clifford S, Cioslowski J, Stefanov BB, Liu G, Liashenko A, Piskorz P, Komaromi I, Martin RL, Fox DJ, Keith T, Al-Laham MA, Peng CY, Nanayakkara A, Challacombe M, Gill PMW, Johnson B, Chen W, Wong MW, Gonzalez C, Pople JA (2004) Gaussian 03. Revision C.02 edn., Wallingford, CT
34. Birk M, Friedl RR, Cohen EA, Pickett HM, Sander SP (1989) The rotational spectrum and structure of chlorine peroxide. J Chem Phys 91(11):6588–6597
35. Becke AD (1993) Density functional thermochemistry. III. The role of exact exchange. J Chem Phys 98(7):5648–5652
36. Lee C, Yang W, Parr RG (1988) Development of the Colle-Salvetti correlation-energy formula into a functional of the electron density. Phys Rev B 37(2):785
37. Vosko SH, Wilk L, Nusair M (1980) Accurate spin-dependent electron liquid correlation energies for local spin density calculations: a critical analysis. Can J Phys 58(8):1200–1211
38. Devlin FJ, Finley JW, Stephens PJ, Frisch MJ (1995) Ab initio calculation of vibrational absorption and circular dichroism spectra using density functional force fields: a comparison of local, nonlocal, and hybrid density functionals. J Phys Chem 99(46):16883–16902
39. Zhao Y, Truhlar DG (2006) A density functional that accounts for medium-range correlation energies in organic chemistry. Org Lett 8(25):5753–5755
40. Frisch MJ, Head-Gordon M, Pople JA (1990) A direct MP2 gradient method. Chem Phys Lett 166(3):275–280
41. Frisch MJ, Head-Gordon M, Pople JA (1990) Semi-direct algorithms for the MP2 energy and gradient. Chem Phys Lett 166(3):281–289
42. Head-Gordon M, Pople JA, Frisch MJ (1988) MP2 energy evaluation by direct methods. Chem Phys Lett 153(6):503–506
43. Head-Gordon M, Head-Gordon T (1994) Analytic MP2 frequencies without fifth-order storage. Theory and application to bifurcated hydrogen bonds in the water hexamer. Chem Phys Lett 220(1–2):122–128
44. Sæbø S, Almlöf J (1989) Avoiding the integral storage bottleneck in LCAO calculations of electron correlation. Chem Phys Lett 154(1):83–89
45. McLean AD, Chandler GS (1980) Contracted Gaussian basis sets for molecular calculations. I. Second row atoms, $Z = 11$–18. J Chem Phys 72(10):5639–5648
46. Krishnan R, Binkley JS, Seeger R, Pople JA (1980) Self-consistent molecular orbital methods. XX. A basis set for correlated wave functions. J Chem Phys 72(1):650–654
47. Davidson ER (1996) Comment on "Comment on Dunning's correlation-consistent basis sets". Chem Phys Lett 260(3–4): 514–518
48. Tomasello P, Ehara M, Nakatsuji H (2003) Theoretical investigation on the valence ionization spectra of Cl_2O, ClOOCl, and F_2O by correlation-based configuration interaction methods. J Chem Phys 118(13):5811–5820
49. Krishnan R, Pople JA (1978) Approximate fourth-order perturbation theory of the electron correlation energy. Int J Quantum Chem 14(1):91–100
50. Purvis GD, Bartlett RJ (1982) A full coupled-cluster singles and doubles model: the inclusion of disconnected triples. J Chem Phys 76(4):1910–1918
51. Scuseria GE, Janssen CL, Schaefer HF (1988) An efficient reformulation of the closed-shell coupled cluster single and double excitation (CCSD) equations. J Chem Phys 89(12): 7382–7387

52. Scuseria GE, Schaefer HF (1989) Is coupled cluster singles and doubles (CCSD) more computationally intensive than quadratic configuration interaction (QCISD)? J Chem Phys 90(7): 3700–3703
53. Hagan MTD, Beale HB (1996) Neural network design. Colorado Bookstore, Boulder, CO
54. Handley CM, Popelier PLA (2010) Potential energy surfaces fitted by artificial neural networks. J Phys Chem A 114(10): 3371–3383
55. Malshe M, Raff LM, Rockley MG, Hagan M, Agrawal PM, Komanduri R (2007) Theoretical investigation of the dissociation dynamics of vibrationally excited vinyl bromide on an ab initio potential-energy surface obtained using modified novelty sampling and feedforward neural networks. II. Numerical application of the method. J Chem Phys 127(13):134105
56. Agrawal PM, Raff LM, Hagan MT, Komanduri R (2006) Molecular dynamics investigations of the dissociation of SiO_2 on an ab initio potential energy surface obtained using neural network methods. J Chem Phys 124(13):134306
57. Le HM, Raff LM (2008) Cis→trans, trans→cis isomerizations and N–O bond dissociation of nitrous acid (HONO) on an ab initio potential surface obtained by novelty sampling and feed-forward neural network fitting. J Chem Phys 128(19):194310
58. Le HM, Huynh S, Raff LM (2009) Molecular dissociation of hydrogen peroxide (HOOH) on a neural network ab initio potential surface with a new configuration sampling method involving gradient fitting. J Chem Phys 131(1):014107
59. Le HM, Raff LM (2009) Molecular dynamics investigation of the bimolecular reaction $BeH + H_2 \rightarrow BeH_2 + H$ on an ab initio potential-energy surface obtained using neural network methods with both potential and gradient accuracy determination. J Phys Chem A 114(1):45–53
60. Le HM, Dinh TS, Le HV (2011) Molecular dynamics investigations of ozone on an ab initio potential energy surface with the utilization of pattern-recognition neural network for accurate determination of product formation. J Phys Chem A 115(40):10862–10870
61. Pukrittayakamee A, Malshe M, Hagan M, Raff LM, Narulkar R, Bukkapatnum S, Komanduri R (2009) Simultaneous fitting of a potential-energy surface and its corresponding force fields using feedforward neural networks. J Chem Phys 130(13):134101
62. Malshe M, Raff LM, Hagan M, Bukkapatnam S, Komanduri R (2010) Input vector optimization of feed-forward neural networks for fitting ab initio potential-energy databases. J Chem Phys 132(20):204103
63. Handley CM, Popelier PLA (2009) Dynamically polarizable water potential based on multipole moments trained by machine learning. J Chem Theory Comput 5(6):1474–1489
64. Caruana R, Lawrence S, Giles CL (2000) Overfitting in neural nets: backpropagation, conjugate gradient, and early stopping. In: Proceedings of neural information processing systems, pp 402–408
65. Malshe M, Narulkar R, Raff LM, Hagan M, Bukkapatnam S, Agrawal PM, Komanduri R (2009) Development of generalized potential-energy surfaces using many-body expansions, neural networks, and moiety energy approximations. J Chem Phys 130(18):184102
66. Agrawal PM, Malshe M, Narulkar R, Raff LM, Hagan M, Bukkapatnum S, Komanduri R (2009) A self-starting method for obtaining analytic potential-energy surfaces from ab initio electronic structure calculations. J Phys Chem A 113(5):869–877
67. MathWorks (2011) MATLAB. Natick, MA
68. Raff LM (1988) Projection methods for obtaining intramolecular energy transfer rates from classical trajectory results: application to 1,2-difluoroethane. J Chem Phys 89(9):5680–5691